



Article

# Power Distribution Strategy for an Electric Bus with a Hybrid Energy Storage System

Yu Zhang <sup>1,2,3</sup>, Kai Li <sup>1,\*</sup>, Shumei Cui <sup>2</sup> and Yutian Sun <sup>3</sup>

<sup>1</sup> College of Electrical and Electronic Engineering, Harbin University of Science and Technology, Harbin 150080, China; zhangyu841998@hrbust.edu.cn

<sup>2</sup> School of Electrical Engineering and Automation, Harbin Institute of Technology, Harbin 150001, China; cuism@hit.edu.cn

<sup>3</sup> Harbin Electrical Machinery Company Limited, Harbin 150040, China; sunyutian@hecchina.com

\* Correspondence: lk9801286926@163.com

**Abstract:** To address the power distribution problem that occurs in hybrid energy storage systems (HESSs) in electric vehicles, a fuzzy control distribution method is proposed in this paper, taking the vehicle demand power; supercapacitor power,  $P_{SC}$ ; and lithium battery power,  $P_{bat}$ , as the inputs and the power distribution factor of the supercapacitor as the output to control the power distribution of the composite energy storage system, in addition to dividing the whole working condition into three time scales, namely, long, medium and short. In this study, we conducted a comprehensive analysis and comparison with typical control methods regarding the energy storage element output power, battery state of charge (SOC) change, energy flow diagram and power frequency. The simulation experiment results show that the proposed strategy is more effective in reducing the peak output power of the power battery, improving the effective power utilization rate of HESS and the effective energy utilization rate. In order to further verify the effectiveness of the control strategy, a pure electric bus power system test bench was built based on similar principles, and a representative time period under the driving conditions of the China city bus (CHTC-B) was selected, involving an acceleration process from 30 to 48 s (process 1), a uniform speed process from 636 to 671 s (process 2) and a regenerative braking process from 1290 to 1304 s (process 3), further verifying the effectiveness and feasibility of the proposed control strategy.

**Keywords:** fuzzy control; HESS; electric bus; power distribution



**Citation:** Zhang, Y.; Li, K.; Cui, S.; Sun, Y. Power Distribution Strategy for an Electric Bus with a Hybrid Energy Storage System. *World Electr. Veh. J.* **2021**, *12*, 154. <https://doi.org/10.3390/wevj12030154>

Academic Editor: Xuhui Wen

Received: 11 July 2021

Accepted: 4 August 2021

Published: 13 September 2021

**Publisher's Note:** MDPI stays neutral with regard to jurisdictional claims in published maps and institutional affiliations.



**Copyright:** © 2021 by the authors. Licensee MDPI, Basel, Switzerland. This article is an open access article distributed under the terms and conditions of the Creative Commons Attribution (CC BY) license (<https://creativecommons.org/licenses/by/4.0/>).

## 1. Introduction

The development of the automobile industry has provided convenience to people, although it has also had adverse effects, such as environmental pollution and greenhouse effects, on the world. Effective solutions are urgently required to alleviate this problem. In [1–4], the authors proposed four energy management strategies to achieve the optimal allocation of required power to reduce consumption. In [5], an optimization method is proposed for energy management strategies based on the principle of the minimum value. In [6], hybrid energy storage systems are used to effectively solve the above problems, showing that the need for related theories and technological breakthroughs is becoming urgent. This paper comprehensively summarizes the key issues regarding the control and management of hybrid energy storage systems from multiple perspectives. In [7], a permanent magnet synchronous motor (PMSM) is used to simulate the traction components of electric vehicles, a new type of fuzzy logic energy management strategy is proposed for a battery–supercapacitor hybrid energy storage system, and its feasibility is verified through experiments. In addition, formulating an optimal control method to optimize vehicle behavior can also effectively solve this problem.

In recent years, intelligent control methods based on neural networks and fuzzy control have also been applied to vehicle energy management technologies, as they are

better than the typical rule-based control method. For the method described in [8], when the fuel consumption rates or emissions are used as the design indicators, the data can be trained on different driving conditions to predict vehicle behavior in the neural network models. In [9], a neural network is used to predict the road conditions and the degree of traffic congestion online and for vehicle energy management. In [10], an effective energy management system for HESS in hybrid electric vehicles is developed based on the concept of a neural network using a closed method. In [11], a neural network is used to manage the energy flow between the energy storage and load in pure electric vehicles and hybrid vehicles. The input of the neural network controller is the output voltage and input current of the converter, while the output signal is controlled by the neural network based on the compared sampling frequency and the adjusting waveform. The fuzzy controller is also used in the vehicle management strategies. In [12], the fuzzy controller is designed to distribute the power between the motor and the engine and to optimize the efficiency of the driving system based on the command, the battery SOC and the motor speed. In [13], the energy flow of a single-axis parallel hybrid vehicle is analyzed using the fuzzy control method. The first input value of the controller is the difference between the required torque and the target torque, which is then negotiated with the required torque, while the second input is the battery SOC. The controller will output the torque control coefficient to distribute the torque between the engine and the motor in real time. Similarly, the fuzzy control is applied to the management of HESS and a fuzzy logic controller is used to distribute the power between the driving system and the energy storage system in [14,15]. In [16], Hu proposes a rule-based adaptive controller based on fuzzy rules by analyzing HESS dynamic programming allocation. Xu and Wang combine supercapacitors with batteries and adopt a parallel interleaving method in a DC/DC converter using the fuzzy control strategy [17], after which the power system greatly improves the overall performance of HESS. In [18,19], Zhou designs a logic threshold control strategy for the HESS of pure electric vehicles. The results show that this control strategy can avoid the large-current impacts and improve the service life of the battery and the driving range of the vehicle. With the deepening of the research, the team applies fuzzy control to the energy management of HESS. In [20], the results prove that fuzzy control can improve vehicle performance. Compared with traditional methods, fuzzy control can obtain better results; however, fuzzy control mainly relies on expert experience, while the rule formulation and membership function both have an impact on the accuracy of the controller.

At present, HESS is attracting increasing attention, and certain success has been achieved in reducing the power consumption and prolonging the service life of batteries. In this paper, we propose a fuzzy control strategy for HESS. A pure electric city bus produced by CENS Energy Tech Co., Ltd. with an HESS was tested, and the drive and energy storage systems were modeled. To optimize vehicle performance, a semi-physical experimental system was designed, and a LabVIEW centralized monitoring control and management system was connected by controller area network communication.

## 2. Establishment of the Vehicle Model

The basic parameters of the target model for Cens Bus are shown in Table 1. According to the experimental conditions, the lithium battery is a Sainz CBP2450lithium-iron phosphate battery, with a nominal voltage of 25.6 V, mass specific power of 1000 W/kg, mass specific energy of 215.49 W·h/kg, nominal capacity of 50 A·h and weight of 19 kg. The single-supercapacitor module uses the BMOD0165 battery produced by MAXWELL in the United States, with a rated voltage of 48 V, peak voltage of 51 V, nominal capacity of 165 F, maximum peak current of 1900 A and nominal weight of 13.5 kg. The rated voltage of the motor is 300 V, the rated power is 120 kW and the rated speed is 1860 r/min.

**Table 1.** Vehicle performance requirements and parameters.

System Parameter		Value
Performance requirements	Maximum speed/(km/h)	$\geq 80$
	Maximum climb/%	$\geq 16$
	Acceleration time/s	$\leq 25$ (0~50 km/h)
	Driving range /km	$\geq 250$ km (Uniform speed 40 km/h)
Vehicle parameter	Size (mm)	12,000 × 2530 × 3080
	No-load mass (kg)	12,000
	Fully loaded quality (kg)	17,800
	Air resistance coefficient $C_d$	0.65
	Rolling resistance coefficient $f_r$	0.0165
	Rolling quality conversion factor	1.08
	Wheel radius (m)	0.469

### 2.1. Vehicle Dynamics Mode

The calculation of the dynamic index is the key to the matching of motor parameters, and it is also an essential step in the initial stage of research and development. It establishes the vehicle dynamics model and obtains the power provided by each energy storage during the control strategy. When an electric vehicle is running, the power battery provides the energy required to overcome various resistances; the electrical energy is converted into the driving force to drive the wheels through the mechanical shaft; and the rotational force output by the motor to the wheels interacts with the frictional force on the ground to produce the traction force, which makes the bus move forward.

The output power of the motor is shown in Formula (1):

$$T = \frac{9.55 \times P}{n} \quad (1)$$

In the formula,  $T$  is the motor output torque, and the unit is  $n.m$ ;  $n$  is the motor speed, and the unit is  $r/min$ ; and  $P$  is the motor output power, and the unit is  $kW$ .

When driving an electric vehicle, the connection between the vehicle and the air produces resistance to the vehicle, and its magnitude is proportional to the square of the speed. The air resistance,  $F_w$ , is shown in Formula (2):

$$F_w = \frac{1}{2} \rho C_d A v^2 \quad (2)$$

In the formula,  $\rho$  is the air density, and the unit is  $kg/m^3$ .  $C_d$  is the coefficient of air resistance.  $A$  is the windward area of the vehicle, and the unit is  $m^2$ .  $v$  is the vehicle's speed, and the unit is  $km/h$ .

The vehicle needs to overcome the effect of additional ramp resistance when it climbs a slope. The greater the slope of the ramp, the better the resistance the vehicle will receive. The calculation method of slope resistance  $F_i$  when climbing is shown in Formula (3):

$$F_i = mg \sin \alpha \quad (3)$$

In the formula,  $m$  is the total weight of the bus,  $g$  is the acceleration due to gravity, and  $\alpha$  is the road slope angle.

When the vehicle is traveling on the road, the frictional resistance of the ground against the wheels can make the vehicle move forward. The friction resistance is related to the rolling friction coefficient between the vehicle and the ground. The formula of rolling friction resistance,  $F_f$ , is shown in (4):

$$F_f = mgC \cos \alpha = mgf \quad (4)$$

In the formula,  $C$  is the coefficient of rolling friction,  $\alpha$  is the road slope angle, and  $f$  is the rolling resistance coefficient.

When a bus is accelerating, it needs to overcome the inertial force generated by its gravity, and its value is related to the rate of speed change.

The acceleration inertia force  $F_j$  is calculated as shown in Formula (5), where  $\delta$  is the conversion factor of rotating mass.

$$F_j = m \cdot \delta \cdot \frac{dv}{dt} \tag{5}$$

The driving force is  $F_t$ , and the equation of motion can obtain from Newton’s second law:

$$F_t - F_f - F_w - F_i = F_j \tag{6}$$

Therefore, the energy  $\Delta E$  required for the vehicle to travel at speed  $v_0$  to speed  $v_1$  can be obtained from the following:

$$\Delta E = \int_{v_0}^{v_1} F_j \cdot v dt + \int_{v_0}^{v_1} F_f \cdot v dt + \int_{v_0}^{v_1} F_w \cdot v dt + \int_{v_0}^{v_1} F_i \cdot v dt \tag{7}$$

$$\Delta E = \int_{v_0}^{v_1} \delta \cdot m \cdot \frac{dv}{dt} \cdot v dt + \int_{v_0}^{v_1} mgf v dt + \int_{v_0}^{v_1} \frac{C_d A v^2}{21.15} \cdot v dt + \int_{v_0}^{v_1} mgv \sin \alpha dt \tag{8}$$

The theoretical calculation model of vehicle driving resistance is shown in Figure 1. Considering the calculation method of speed in CRUISE, the average value of adjacent sampling points is selected when calculating the speed inside the model. It supposes that the speeds of adjacent sampling points are  $v_{end}$  and  $v_{sta}$ , and the average speed is  $v_{ave}$ . The speed conversion model is shown in Figure 2.

$$v_{ave} = (v_{end} + v_{sta})/2 \tag{9}$$

$$v_{end} = 2 \cdot v_{ave} - v_{sta} \tag{10}$$

$$a = dv/dt = (v_{end} - v_{sta})/(t_{end} - t_{sta}) = 2 \cdot (v_{ave} - v_{sta})/dt \tag{11}$$

Therefore, the resultant force has the following formula:

$$2\delta m(v_{ave} - v_{sta})/dt + mgf + \frac{C_d \cdot A \cdot (2v_{ave} - v_{sta})^2}{21.15} + mg \sin \alpha - F_t = 0 \tag{12}$$

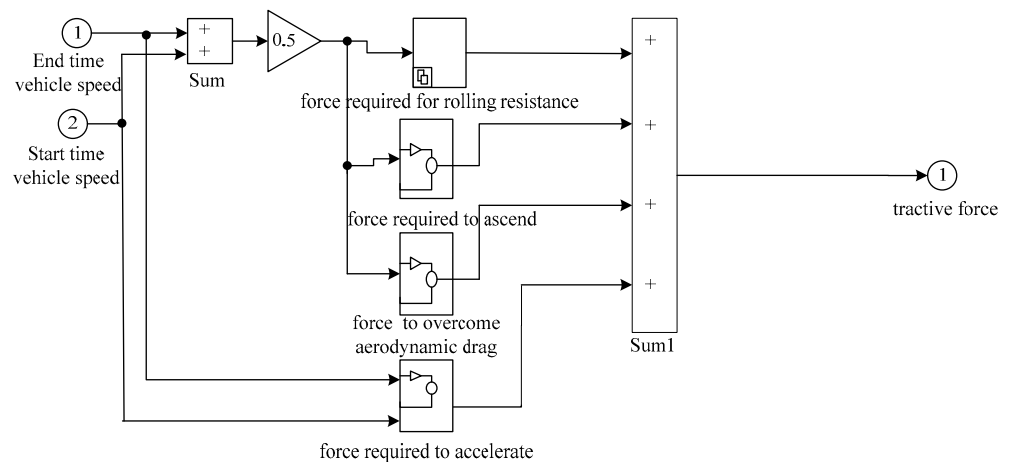


Figure 1. Vehicle resistance calculation model.

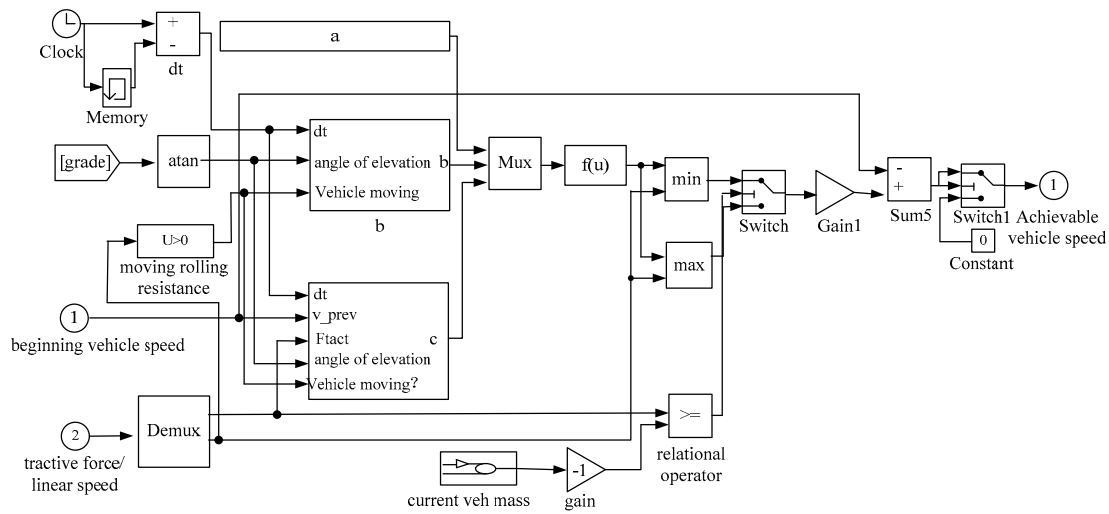


Figure 2. Speed calculation model.

In the velocity calculation model:

$$a = 4C_d \cdot A/21.15 \tag{13}$$

$$b = 2(\delta m/dt - 2v_{sta}/21.15) \tag{14}$$

$$c = mg \sin \alpha + mgf + C_d A v_{sta}^2/21.15 - 2\delta m v_{sta}/dt - F_t \tag{15}$$

For the speed conversion model created under braking, the idea is the same, and the current speed should also be required in extreme situations, such as sideslip.

### 2.2. Power Calculation and Distribution Model for HESS

The topology of HESS chooses a semi-active topological structure in which the supercapacitor is connected in series with bi-directional DC-DC and then connected in parallel with lithium batteries. In the case of parameter matching to meet the requirements of the working conditions, the reverse direction starts from the required power output by each energy storage element; since the energy storage components on electric buses have a relatively large mass and consume more power and energy, the power consumption caused by their mass is introduced into the model construction; combining the modular modeling idea, it calculates the fuel economy, emission, power, gearbox ratio, braking performance, etc., of the vehicle according to the structural layout of the experimental prototype. Table 2 shows the connection between the models in CRUISE.

Table 2. The connection between the models in CRUISE.

Link Mode	Mechanical Link	Emission Link	Electrical Link	Data Bus Information Terminal
model				

According to the link mode of the mechanical, electrical and data bus between the various components of the pure electric city bus, the joint simulation model of the pure electric city bus of the compound energy storage system can be established. This thesis takes the Sainz pure electric bus as the prototype, builds the primary component model in MATLAB, and realizes the co-simulation through a variable link. The HESS model uses MATLAB 2014 a and CRUISE (60-day trial version) to work together. MATLAB DLL is used in the communication between MATLAB and CRUISE, and it needs to create a

dynamic link library to generate DLL files after building the model in Simulink, which is faster than the MATLAB API simulation speed.

Adding the constructed HESS model to the CRUISE module component library can quickly realize the complex energy simulation of various topologies. The DC/DC converter model in CRUISE can learn the unidirectional flow of current from the high-voltage side to the low-voltage side or from the low-voltage side to the high-voltage side by switching the SWITCH signal. In Figure 3, the HESS power decoupling distribution process is shown. According to the speed model and the resistance model, the total demand power can be obtained. The outputs of the super-capacitor and the battery are obtained from the control method of Mallat continuation Hal wavelet power decoupling power.

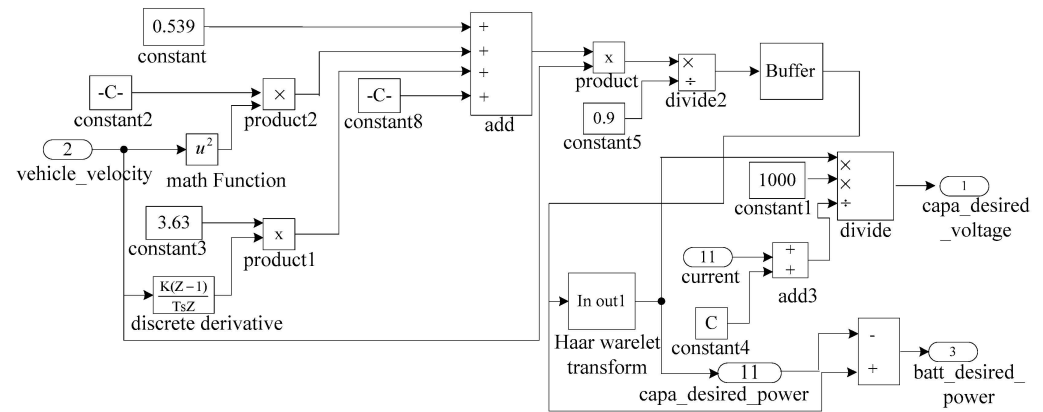


Figure 3. Power distribution process of HESS.

Figure 4 shows the power calculation model of energy storage. In the case of bi-directional DC/DC current control, the terminal voltage value can be obtained, and the dual-energy sources jointly overcome the power consumption caused by rolling friction resistance, climbing resistance and acceleration resistance during the traveling process.

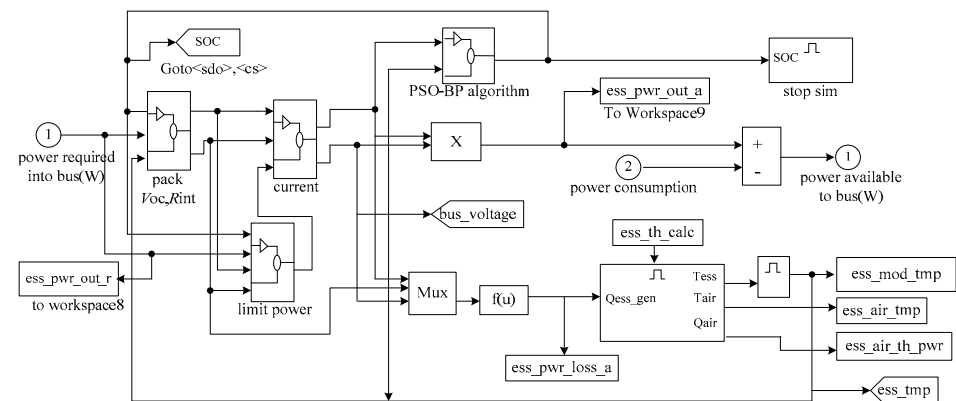


Figure 4. HESS energy storage power calculation model.

The construction of the vehicle model was carried out under the environment of CRUISE-MATLAB. For the construction of the dynamic model, first, the power demand of the vehicle during driving was calculated. Then, the acceleration, maximum speed and maximum grade of the vehicle were calculated to match the energy storage capacity; that is to say, the dynamic model was created from the reverse perspective, as it takes the required power as the input signal. This study constructed a dual closed-loop human-machine dynamics coupling model of a pure electric bus, in which the vehicle dynamics system is a time-varying system, and the control method is an outer loop control; the vehicle dynamics system issues a command to the electric drive system according to demand,

and the drive motor meets the torque and rotating speed requirements of the electric bus and transmits energy with the energy storage system; it belongs to the inner loop control, and the two together form a dual closed-loop control [21,22]. In CRUISE, the internal electrical and mechanical parts of the composite energy storage system are, and the vehicle dynamics model was built. This provides a good foundation for subsequent co-simulation and strategy research.

The vehicle model establishment relationship diagram is shown in Figure 5.

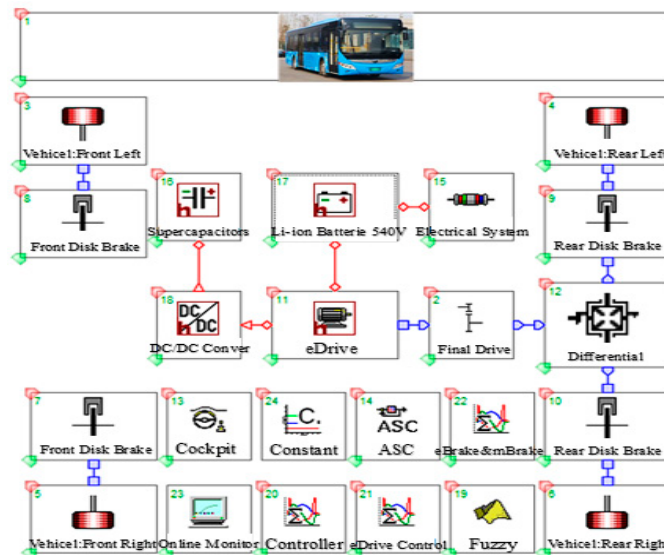


Figure 5. Vehicle model establishment relationship diagram.

Compared with other models, the electric passenger bus has a larger mass, and the matched energy storage components are connected in series and parallel through the modules. Whilst driving, the whole vehicle needs to overcome the climbing resistance, acceleration resistance and rolling resistance caused by its mass, and the resulting power loss is very large; the self-consumption model was introduced into the construction of the HESS model. The input current signal of the created model was compared with the voltage signal obtained through the simulation and experiment. The results show that the error is within 2%, which also proves the correctness of the simulation model.

### 3. Design of Fuzzy Controller

To meet the driving demand, the design needs to reasonably allocate the power output ratio of the super-capacitor and the lithium battery, and the power of the super-capacitor and the lithium battery should satisfy the relationship shown in Formula (16).

$$P_{\text{req}} = P_{\text{SC}} + P_{\text{bat}} \quad (16)$$

$K_{\text{SC}}$  is the super-capacitor power distribution factor, which represents the ratio of the super-capacitor power,  $P_{\text{SC}}$ , to the pure electric bus demand power,  $P_{\text{req}}$ , and its expression is shown in Formula (17).

$$P_{\text{SC}} = P_{\text{req}} \cdot K_{\text{SC}} \quad (17)$$

Therefore, the output of the hybrid energy storage system is mainly related to the required power,  $P_{\text{req}}$ ; super-capacitor power,  $P_{\text{SC}}$ ; and lithium battery power,  $P_{\text{bat}}$ , of pure electric buses, and the power of super-capacitors and lithium batteries is closely related to their state of charge. Therefore, the input of the fuzzy controller is set to the state of charge,  $S_{\text{SOC}}$ , of the super-capacitor; the state of charge,  $B_{\text{SOC}}$ , of the lithium battery; and the required power,  $P_{\text{req}}$ , of the pure electric bus, and the output of the fuzzy controller is set to the power distribution factor  $K_{\text{SC}}$  of the super-capacitor. When the pure electric passenger bus is in the state of starting, accelerating, climbing or driving at a constant

speed, the fuzzy controller distributes the output of the super-capacitor and the lithium battery; when the pure electric passenger bus is in the deceleration or braking state, the super-capacitor is the primary energy storage device for energy recovery, and the recovery method is the same as that of the logic threshold control strategy. When a pure electric bus is running normally, if the super-capacitor terminal voltage is lower than its standard working voltage, the lithium battery can adequately charge the super-capacitor when its output power is low.

When the motor is in the driving state, the demand power,  $P_{req}$ , of the pure electric passenger bus is greater than zero. The domain of the membership function of the pure electric bus demand power,  $P_{req}$ , in the interval was set [0,1], and the interval was divided into five subsets:  $P_{req} = \{TL, L, M, H, TH\}$ ; the membership function of the demand power of a pure electric bus is shown in Figure 6. The membership function domain of the lithium battery power,  $P_{bat}$ , in the interval was set [0,1], and the interval was divided into three subsets:  $B_{SOC} = \{L, M, H\}$ ; the membership function of lithium battery power is shown in Figure 7.

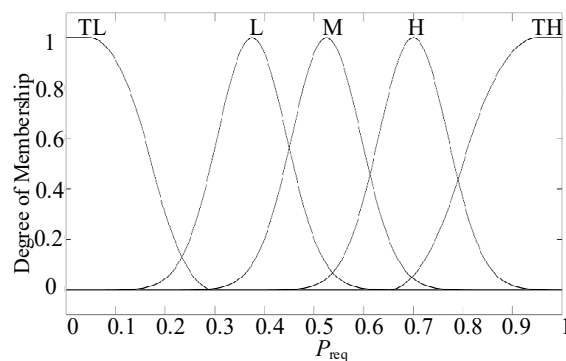


Figure 6. Membership function of  $P_{req}$ .

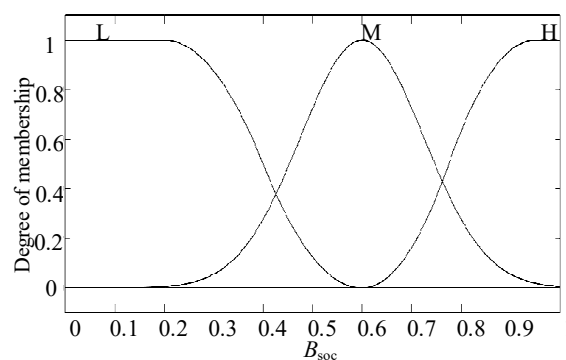


Figure 7. Membership function of  $B_{SOC}$ .

The membership function domain of the super-capacitor's state of charge,  $S_{SOC}$ , in the interval was set (0.1,1), and the interval was divided into three subsets:  $S_{SOC} = \{L, M, H\}$ ; the membership function of the  $S_{SOC}$  of the super-capacitor state of charge is shown in Figure 8. The membership function domain of the supercapacitor's power distribution factor,  $K_{SC}$ , in the interval was set (0.1,1), and the interval was divided into five subsets:  $K_{SC} = \{TL, L, M, H, TH\}$ ; the membership function of the super-capacitor power distribution factor is shown in Figure 9.

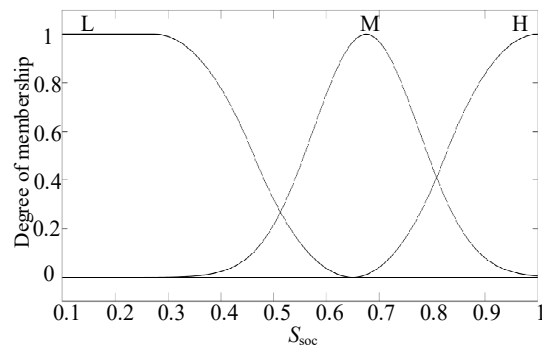


Figure 8. Membership function of  $S_{SOC}$ .

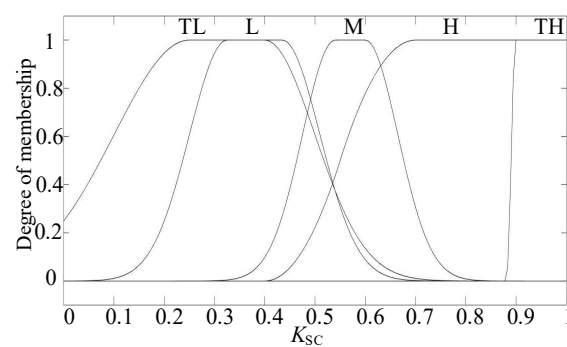


Figure 9. Membership function of  $K_{SC}$ .

Based on the four membership functions formulated above, forty-five fuzzy control rules were designed; the specific rules are shown in Tables 3–5.

Table 3. Fuzzy control rules ( $S_{SOC} = L$ ).

$K_{SC}$		$B_{SOC}$		
		L	M	H
$P_{req}$	TL	TL	TL	TL
	L	TL	TL	TL
	M	TL	TL	TL
	H	L	TL	TL
	TH	L	L	TL

Table 4. Fuzzy control rules ( $S_{SOC} = M$ ).

$K_{SC}$		$B_{SOC}$		
		L	M	H
$P_{req}$	TL	TL	TL	TL
	L	L	TL	TL
	M	M	L	TL
	H	H	M	M
	TH	H	H	H

According to the four membership functions designed above and forty-five fuzzy control rules, the state of charge,  $S_{SOC}$ , of the super-capacitor; the state of charge,  $B_{SOC}$ , of the lithium battery; and the relationship between the required power,  $P_{req}$ , of a pure electric bus and the power distribution factor,  $K_{SC}$ , of the super-capacitor can be obtained; the input–output relationship surface obtained in MATLAB is shown in Figure 10.

**Table 5.** Fuzzy control rules ( $S_{SOC} = H$ ).

		$K_{SC}$	$B_{SOC}$		
			L	M	H
$P_{req}$	TL	L	TL	TL	
	L	M	L	TL	
	M	H	M	L	
	H	TH	H	M	
	TH	TH	TH	H	

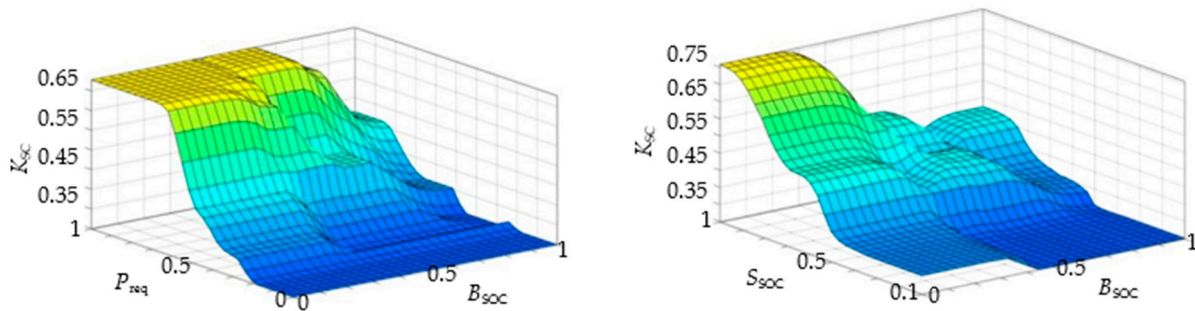


**Figure 10.** Relationship among  $S_{SOC}$ ,  $B_{SOC}$ ,  $P_{req}$  and  $K_{SC}$ .

When converting the fuzzy output into the precise output, the center of gravity method, the weighted average method, the maximum membership method or the membership limit element average method can generally be used; this paper used the weighted average method, and the calculation formula is shown in Formula (18).

$$x_0 = \frac{\sum_{i=1}^n x_i \mu_U(x_i)}{\sum_{i=1}^n \mu_U(x_i)} \tag{18}$$

where  $U$  is the fuzzy output set;  $\mu_U(x_i)$  is the membership function;  $x_0$  is the result after defuzzification.

**4. Simulation Results Analysis**

The proposed control method was applied to the experimental prototype under the China city road cycle. The simulation experiment results of the HESS pure electric bus and the pure electric bus were analyzed and compared with a single lithium battery as the energy storage. The corresponding relationship between the working condition time and speed of China city road cycle is shown in Figure 11. The detailed driving condition information includes the total driving time of 1306 s, the average speed of 16.1 km/h, the maximum speed of 60 km/h, the average driving speed of 16.27 km/h, the total mileage of 5.84 km, the average acceleration of 0.3 m/s<sup>2</sup>, the maximum acceleration of 0.91 m/s<sup>2</sup>, the maximum deceleration of -1.04 m/s<sup>2</sup>, the average deceleration of -0.42 m/s<sup>2</sup>, the idling time of 366 s, the number of starts and stops of 13 times and the required energy of 7.26 kW·h. The corresponding demand power under the China city road cycle is shown in Figure 12. It can be seen from the figure that there are more power spikes, the maximum power is 165.312 kW, the minimum is -153.85 kW and the maximum change in power is 319.162. kW; the power changes significantly at the start and stop moments. Under a single experimental road condition, the power emitted and absorbed by the super-capacitor was 32.85 and 33.08 kW, respectively, and the power emitted and absorbed by the battery was 30.86 and 16.97 kW, respectively. In the process of energy recovery, the super-capacitor recovered more power and absorbed more energy.

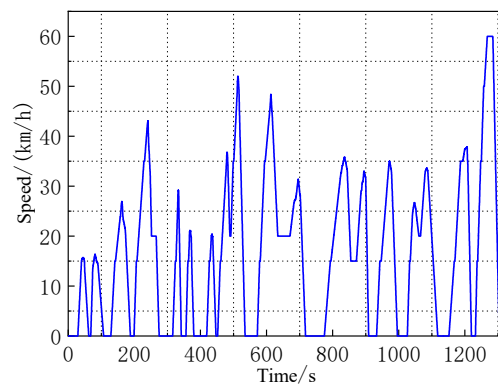


**Figure 11.** The information of China city road cycle.

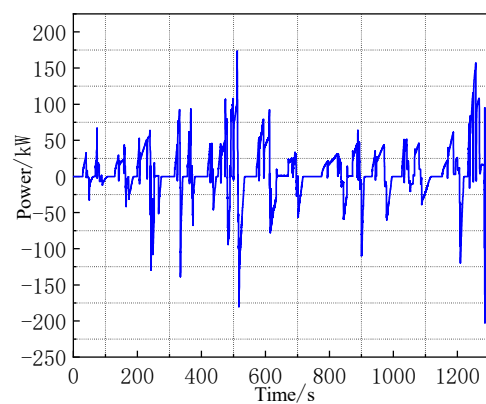


**Figure 12.** The required power of China city road cycle.

When the lithium battery was powered alone, the maximum current of the lithium battery was 313.73 A, the maximum power was 176.10 kW and the output of the lithium battery was too high; when it used the fuzzy control strategy, the maximum current of the lithium battery was 62.29 A and the maximum power was 35.06 kW; the output current and power of the battery reduced drastically. The power demand of the pure electric bus exceeded the maximum power of the bi-directional DC/DC converter during the driving process; the remaining power could only be provided by the lithium battery to meet the driving demand, and the maximum power of the lithium battery was generated at this time, as shown in Figures 13–16.

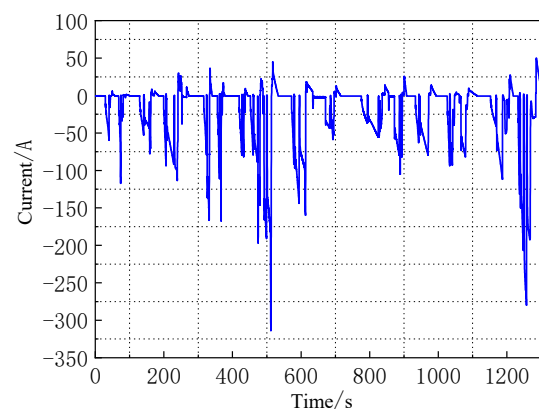


**Figure 13.** Current when battery is powered alone.

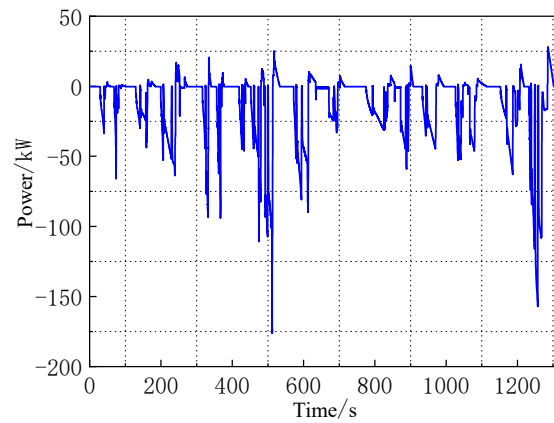


Figure 14. Power when battery is powered alone.

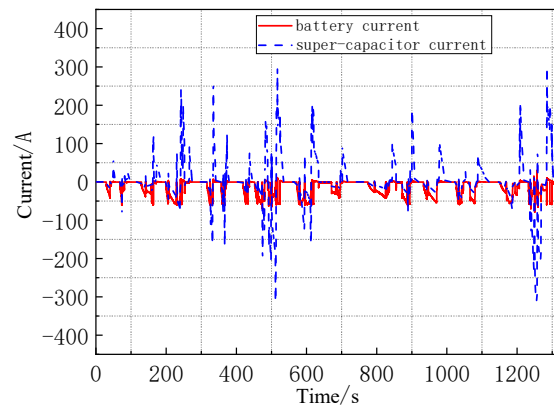


Figure 15. HESS current when using fuzzy control.

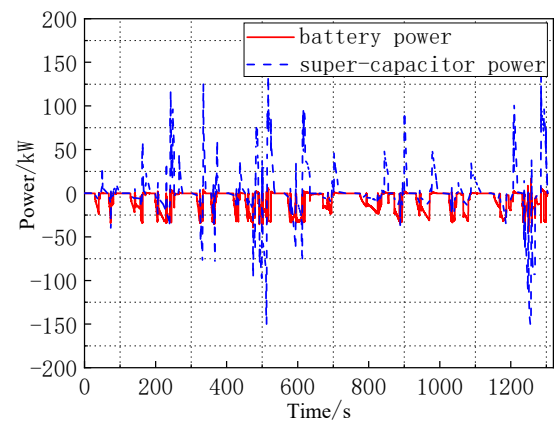


Figure 16. HESS power when using fuzzy control.

From the perspective of energy flow, we analyze the simulation results. From Figures 17 and 18, it can be seen that when the lithium battery alone provided energy for the motor, the lithium battery consumed 4.64 kWh and the reclaimed braking energy was 0.48 kWh; when adopting fuzzy control at the same time, the composite energy storage system consumed 2.86 kWh of energy and recovered 2.70 kWh of braking energy.

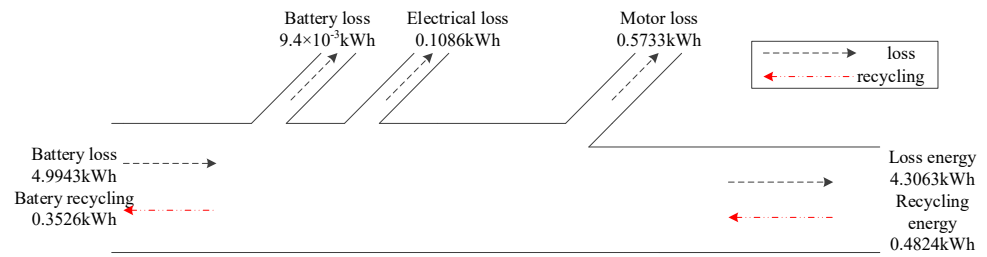


Figure 17. Energy flow chart of lithium battery as a single energy source.

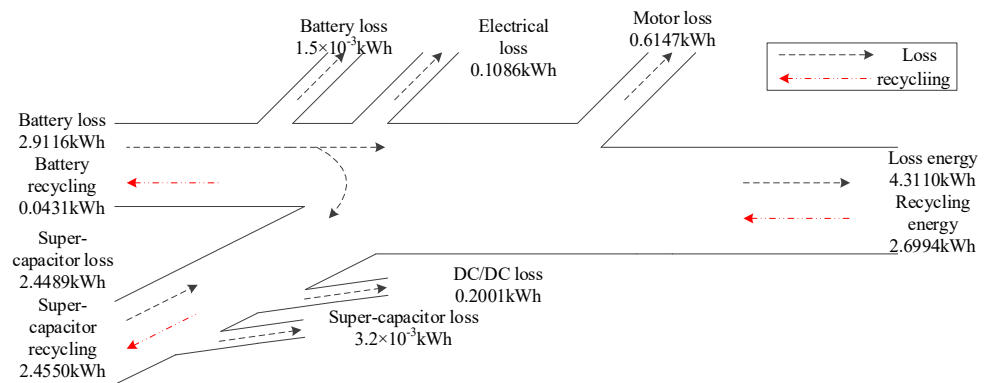


Figure 18. Energy flow diagram with fuzzy control strategy.

### 5. Analysis on the Experiment Results

#### 5.1. Experimental Platform Construction

According to the topology of the prototype, the experimental platform was constructed. The super-capacitor is connected in the branch circuit. The opening and closing of IGBT in bi-directional DC/DC will affect the punctuality and accuracy of the energy transfer between HESS. The drive circuit, voltage and current sampling circuit, protection circuit and auxiliary power supply circuit were designed. The HESS hardware components of the experimental bench are the same lithium battery and super-capacitor module of the prototype. The rules are shown in Formula (19), in which  $\Pi_1$  and  $\Pi_2$  are the criteria, and the similar distortions and equivalent errors are within the allowable range.

$$f\left(\prod_1, \prod_2, \dots\right) = f\left(\frac{P_{batt}}{m_{batt}}, \frac{P_{capa}}{m_{capa}}, \frac{u_R}{i \cdot R}, \frac{u_L \cdot t}{L \cdot i}, \frac{u_C \cdot C}{i \cdot t}, \dots\right) = 0 \quad (19)$$

According to the actual speed requirement of typical working conditions, the actual power requirement was calculated by the vehicle demand model in Labview. According to the control algorithm, the power allocation between the lithium battery and the super-capacitor was carried out. The electric signal collected by the PCI-1716 L card was transmitted to the industrial control computer, and the output control signal was sent to the DC/DC controller through CAN communication. The hardware circuit design and host computer interface are shown in Figure 19.

#### 5.2. Comparative Analysis of Experimental Results

For the convenience of detailed analysis, a representative time period under Chinese city road conditions was selected: acceleration process from 30 to 48 s (Process 1), constant speed process from 636 to 671 s (Process 2) and regenerative braking process from 1290 to 1304 s (Process 3). According to the power level of the experimental platform, the required power under the same simulation conditions was calculated.

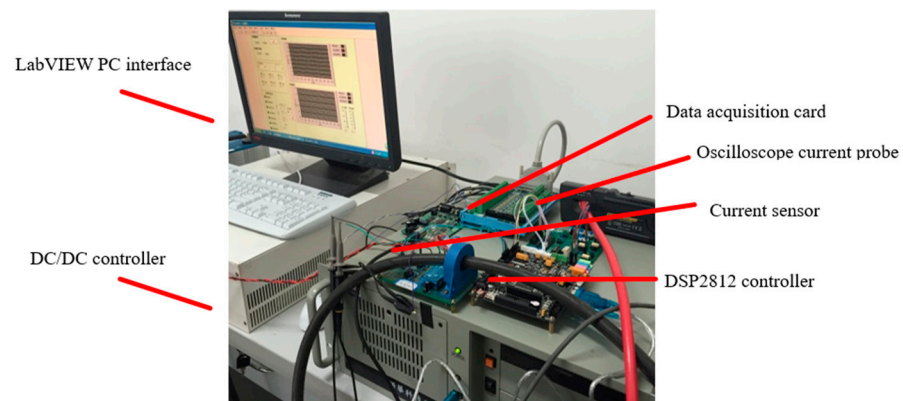


**Figure 19.** Hardware circuit design and host computer interface.

During the experiments, data were collected mainly through the interface of the host computer, and an oscilloscope was used to monitor and compare at the same time. The loading mode of the dynamometer was set to power loading, and the sampling point interval was set to 250 ms. At the same time, the motor speed was adjusted to synchronize the speed with the load demand power.

Before 29 s,  $v = 0$  km/h, the battery charged the super-capacitor until the two voltages were nearly equal and the voltage reached the theoretical reference value. In this case, the working efficiency of DC/DC was improved; Figures 20 and 21 show the voltage changes in the high-voltage end and the low-voltage end. The voltage of the battery also dropped, which proves that the frequency division control strategy is effective and feasible.

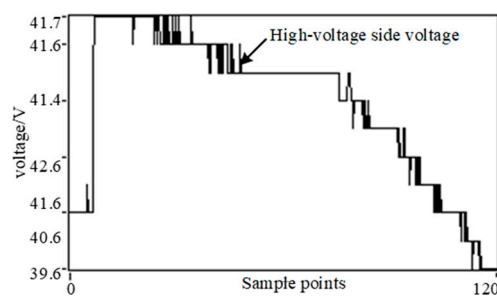


**Figure 20.** High-voltage terminal voltage.

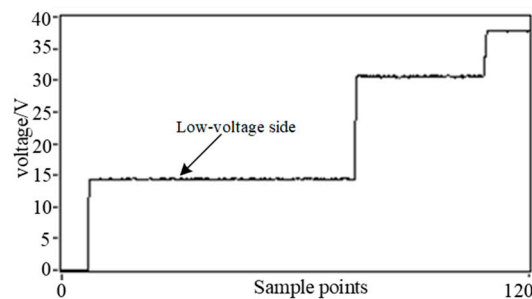


**Figure 21.** Low-voltage terminal voltage.

The corresponding vehicle speed was 20 km/h when the road surface with a simulated slope angle of 10% ran at a constant speed. At the beginning of the uniform speed process, the super-capacitor is still the main power supply, as the required power stabilizes, the battery becomes the main source of energy, and the output current is stable, as shown in Figures 22 and 23.

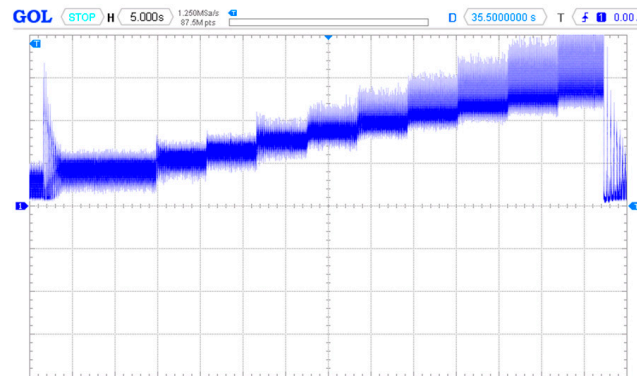


Figure 22. Motor controller current when climbing with constant speed.

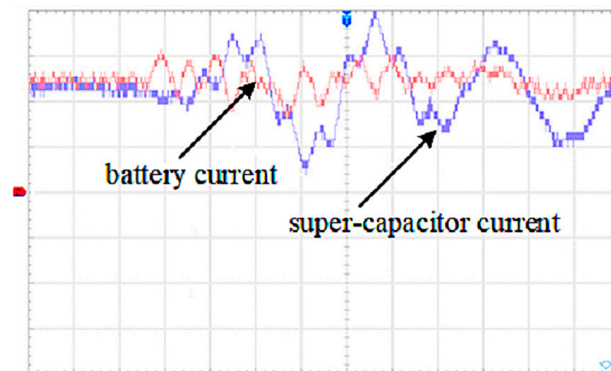


Figure 23. Battery and super-capacitor currents when climbing with constant speed.

Figure 24 shows the power change in the super-capacitor during the acceleration experiments. It can be seen that the instantaneous peak of power exists and is very large. The voltage and current were collected by the sensor and filtered to obtain the corresponding proportional coefficient. Additionally, it can be seen from the power distribution diagram in Figure 25 that the lithium batteries were distributed in the low output power area, and the changing trend of the distribution points was relatively flat and densely distributed in a wide range of positive load required power. This changing trend is also in accordance with the actual driving conditions of acceleration.

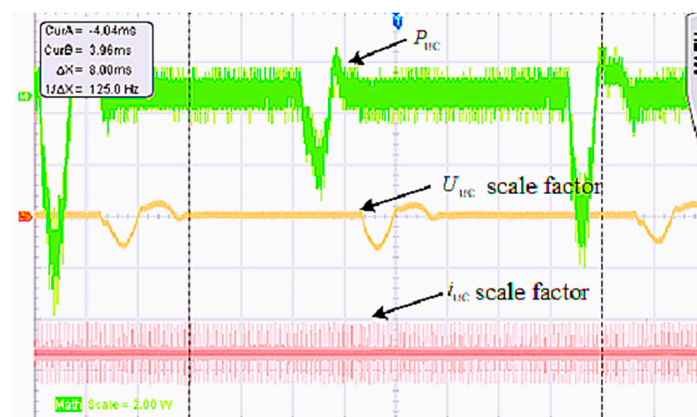


Figure 24. Super-capacitor power–voltage–current variation when accelerating.

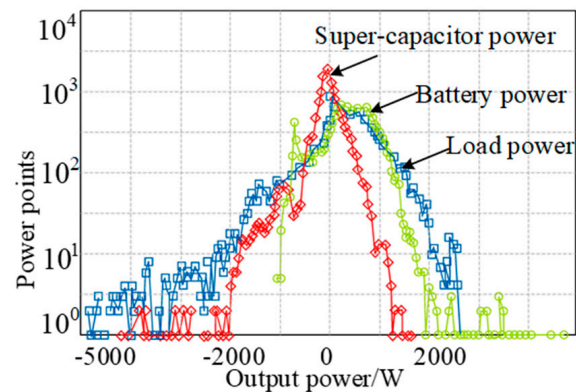


Figure 25. Experimental data power distribution points.

During the braking process, the reverse DC current bus voltage generated at the motor controller terminal increased sharply, as shown in Figure 26. Figure 27 shows the waveform diagram after inverting the feedback current of the super-capacitor and the battery. In the figure, the braking current recovered by the super-capacitor has a larger peak value and a higher rate of change. The instantaneous large current was continuously recovered; however, the instantaneous frequency of the dynamic battery current was small.

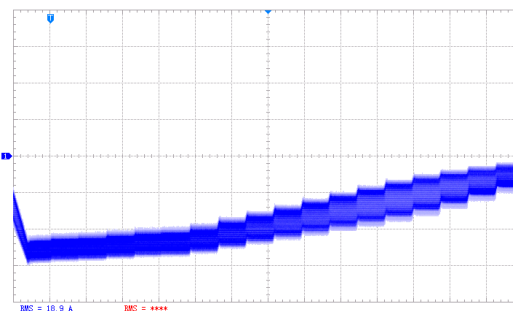


Figure 26. Motor controller bus current when braking.

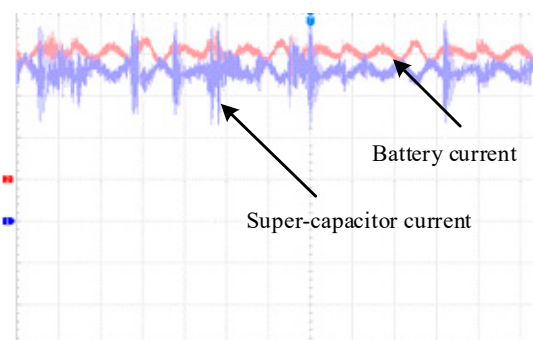
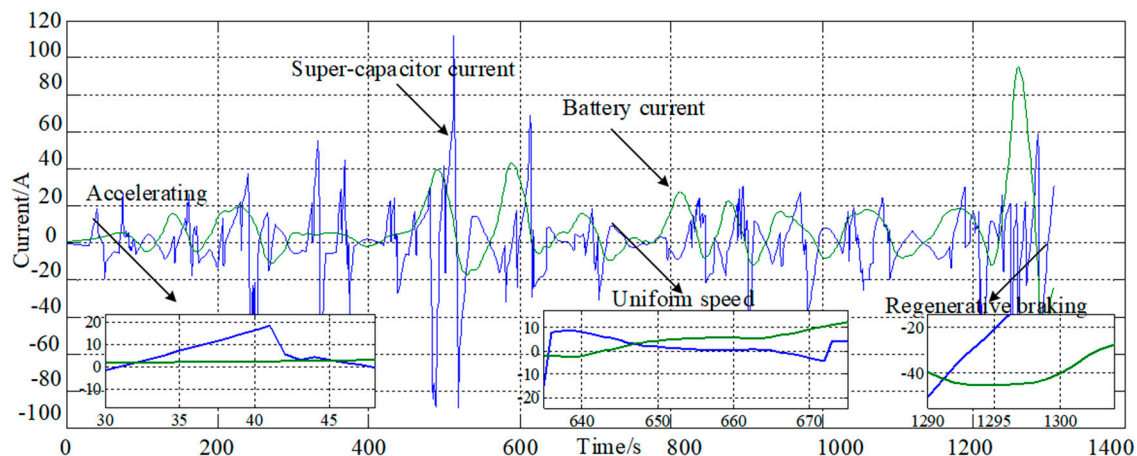


Figure 27. Battery and super-capacitor currents.

Based on the above experimental analysis, in the proposed control method, the current changes in the battery and the super-capacitor are shown in Figure 28. It can be seen that the super-capacitor plays a good role in peak shaving and valley filling; the charge–discharge current of the battery is stable during the acceleration, uniform velocity and braking of the vehicle; the above experimental curve is compared with the current waveform, and the changing trend of the experimental and simulation results is the same.



**Figure 28.** The battery and super-capacitor current response during the whole road cycle.

## 6. Conclusions

Aiming to overcome the problems of poor power performance and short driving range of traditional pure electric buses, bidirectional DC/DC and super capacitor branches were added to a pure electric bus power supply system to form a composite energy storage system. This paper used a fuzzy control method. The experimental results show that the addition of a super-capacitor dramatically reduces the current of lithium battery. Under typical urban road cycling conditions in China, compared with lithium batteries alone providing energy, the fuzzy control strategy saves 1.78 kWh electricity per cycle. It can be proved that the formulated energy control strategy can significantly reduce the charging and discharging current of the lithium battery and effectively recover the braking energy of the motor.

**Author Contributions:** Writing—original draft preparation, Y.Z., S.C. and Y.S.; writing—review and editing, K.L. All authors have read and agreed to the published version of the manuscript.

**Funding:** This work was supported by the Natural Science Foundation of China (grant no.51877057) and Industry-Education Cooperation Collaborative Education Funding Project (grant no.201902273013).

**Conflicts of Interest:** The authors declare no conflict of interest.

## References

- Zhang, Y.; Guo, C.; Li, G.; Liu, Y.; Chen, Z. Cooperative control strategy for plug-in hybrid electric vehicles based on a hierarchical framework with fast calculation. *J. Clean. Prod.* **2020**, *251*, 119627. [[CrossRef](#)]
- Hu, J.; Jiang, X.; Jia, M. Energy Management Strategy for the Hybrid Energy Storage System of Pure Electric Vehicle Considering Traffic Information. *Appl. Sci.* **2018**, *8*, 1266. [[CrossRef](#)]
- Ming, L.; Bo, H.; Shuaishuai, G.; Huan, W. Research on Energy Management and Mode Switching Control of Parallel Hybrid Electric Vehicle. *J. Nanjing Univ. Sci. Technol.* **2020**, *44*, 696–704.
- Yang, C.; You, S.; Wang, W.; Li, L.; Xiang, C. A Stochastic Predictive Energy Management Strategy for Plug-in Hybrid Electric Vehicles Based on Fast Rolling Optimization. *IEEE Trans. Ind. Electron.* **2020**, *67*, 9659–9670. [[CrossRef](#)]
- Feng, L.; Zhongping, Y.; Yun, W.; Xingkun, A.; Fei, L. Energy management strategy of hybrid energy storage tram based on Pontryagin's minimum principle. *Trans. Chin. Soc. Electr. Eng.* **2019**, *34*, 752–759.
- Wang, Y.; Wang, L.; Li, M.; Chen, Z. A review of key issues for control and management in battery and ultra-capacitor hybrid energy storage systems. *eTransportation* **2020**, *4*, 100064. [[CrossRef](#)]
- Sellali, M.; Abdeddaim, S.; Betka, A.; Djerdir, A.; Drid, S.; Tiar, M. Fuzzy-Super twisting control implementation of battery/super capacitor for electric vehicles. *ISA Trans.* **2019**, *95*, 243–253. [[CrossRef](#)] [[PubMed](#)]
- Murphey, Y.L.; Park, J.; Kiliaris, L. Intelligent hybrid vehicle power control-Part II: Online intelligent energy management. *IEEE Trans. Veh. Technol.* **2013**, *62*, 69–79. [[CrossRef](#)]
- Millo, F.; Rolando, L.; Mallamo, F.; Fuso, R. Development of an optimal strategy for the energy management of a range-extended electric city bus with additional noise, vibration and harshness constraints. *J. Automob. Eng.* **2013**, *227*, 4–16. [[CrossRef](#)]

10. Marie, J.N.; Gualous, H.; Berthon, A. DC to DC converter with neural network control for on-board electrical energy management. In Proceedings of the 4th International Power Electronics and Motion Control Conference, Xian, China, 14–16 August 2004; Volume 2, pp. 521–525.
11. Wai, C.L.; Wan, W.Y.; Kumar, R.R. Hybrid energy storage systems and control strategies for stand-alone renewable energy power systems. *Renew. Sustain. Energy Rev.* **2016**, *66*, 174–189.
12. Dawei, M.; Yu, Z.; Meilan, Z.; Risha, N. Intelligent fuzzy energy management research for a uniaxial parallel hybrid electric vehicle. *Comput. Electr. Eng.* **2016**, *58*, 447–464. [[CrossRef](#)]
13. Carter, R.; Cruden, A.; Hall, P.J.; Zaher, A.S. An improved lead acid battery pack model for use in power simulations of electric vehicles. *IEEE Trans. Energy Convers.* **2012**, *27*, 21–28. [[CrossRef](#)]
14. Khayyam, H. Stochastic Models of road geometry and wind condition for vehicle energy management and control. *IEEE Trans. Veh. Technol.* **2013**, *62*, 61–68. [[CrossRef](#)]
15. Penglong, S.; Zhumu, F. Regenerative Braking Fuzzy Control Strategy for CVT HEV. *J. Comput. Simul.* **2014**, *31*, 210–214.
16. Snoussi, J.; Elghali, S.B.; Benbouzid, M. Auto-Adaptive Filtering-Based Energy Management Strategy for Fuel Cell Hybrid Electric Vehicles. *Energies* **2018**, *11*, 2118. [[CrossRef](#)]
17. Zhang, X.; Lu, Z.; Lu, M. Vehicle Speed Optimized Fuzzy Energy Management for Hybrid Energy Storage System in Electric Vehicles. *Complexity* **2020**, *2020*, 2073901. [[CrossRef](#)]
18. Meilan, Z.; Jifeng, F.; Yu, Z. Research on Power Allocation Control Strategy For Compound Electric Energy Storage System of Pure Electric Bus. *Trans. China Electrotech. Soc.* **2019**, *34*, 5001–5013.
19. Meilan, Z.; Jifeng, F.; Yu, Z. Composite energy storage system and its energy control strategy for electric vehicles. *Electr. Mach. Control.* **2019**, *23*, 51–59.
20. Wang, Y.; Wang, W.; Zhao, Y.; Yang, L.; Chen, W. A Fuzzy-Logic Power Management Strategy Based on Markov Random Prediction for Hybrid Energy Storage Systems. *Energies* **2016**, *9*, 25. [[CrossRef](#)]
21. Cong, Z.; Haitao, M.; Yuanbin, Y. Using CPE Function to Size Capacitor Storage for Electric Vehicles and Quantifying Battery Degradation during Different Driving Cycles. *Energies* **2016**, *9*, 903.
22. Hemmati, R.; Saboori, H. Emergence of hybrid energy storage systems in renewable energy and transport applications—A review. *Renew. Sustain. Energy Rev.* **2016**, *65*, 11–23. [[CrossRef](#)]